AIP Journal of Applied Physics

Near-field mapping of dipole nano-antenna-coupled bolometers

Eric Tucker, Jeffrey D' Archangel, Markus Raschke, Edgar Briones, Francisco Javier González, and Glenn Boreman

Citation: Journal of Applied Physics **114**, 033109 (2013); doi: 10.1063/1.4815882
View online: http://dx.doi.org/10.1063/1.4815882
View Table of Contents: http://scitation.aip.org/content/aip/journal/jap/114/3?ver=pdfcov
Published by the AIP Publishing

JOURNAL OF APPLIED PHYSICS **114**, 033109 (2013)

Near-field mapping of dipole nano-antenna-coupled bolometers

Eric Tucker,[1] Jeffrey D' Archangel,[2] Markus Raschke,[3] Edgar Briones,[4]
Francisco Javier González,[4] and Glenn Boreman[1,a)]
[1]*Department of Physics and Optical Science, University of North Carolina at Charlotte, Charlotte, North Carolina 28223, USA*
[2]*CREOL, The College of Optics and Photonics, University of Central Florida, Orlando, Florida 32816, USA*
[3]*Department of Physics, Department of Chemistry, and JILA University of Colorado, Boulder, Colorado 80309, USA*
[4]*Coordinación para la Innovación y la Aplicación de la Ciencia y la Tecnología, Universidad Autónoma de San Luis Potosí, SLP, Mexico*

(Received 26 May 2013; accepted 28 June 2013; published online 18 July 2013)

The near-field characteristics of single, double, and arrays of connected dipole nano-antennas coupled to bolometers were studied by infrared scattering scanning near-field optical microscopy (*s*-SNOM) and analyzed by numerical simulations. Results were consistent with classical antenna theory showing the expected π phase difference across the terminals of the dipoles. However, according to the observed differences between the measurements and simulations, the symmetry of the amplitude signal appeared to be sensitive with respect to the position of the bolometric element relative to the dipoles. The effect of the position of the bolometer on the associated near-field distribution suggests an influence on the coupling and efficiency of energy transfer into these detectors, which could be important for determining tolerances in the fabrication of such devices. These results show how near-field measurements in general can provide critical information to guide the design of nano-antennas, nano-antenna-phased arrays, and integrated photonic devices. [http://dx.doi.org/10.1063/1.4815882]

I. INTRODUCTION

Antenna-coupled bolometers use nano-antennas to couple electromagnetic energy in the visible and infrared regions of the spectrum into high frequency currents, which increase the temperature of the bolometric element placed at the feed of the nano-antenna through Joule heating. This increase in temperature results in a change of resistance which can be measured and correlated to the amount of radiation incident on the nano-antenna.[1,2]

These nano-antenna-based bolometric detectors have potential advantages over traditional far-infrared detectors due to their faster response times, increased responsivity, wavelength selectivity, and polarization sensitivity.[2,3] Advances in the fabrication and measurement of these devices make their application in different regions of the electromagnetic spectrum possible.[1]

Previous work has reported promising results on the use of various planar nano-antenna geometries for long-wave infrared detection (~10 μm),[4–9] however, all the measurements were performed exclusively in the *far-field*. However, excitation and energy transfer to the bolometric element are largely dictated by the local near-field properties of the antenna. Therefore, in order to understand and improve the antenna-bolometer coupling, probing of the spatial near-field distribution is highly desirable.

Scattering-type scanning *near-field* optical microcopy (*s*-SNOM) has proven to be a powerful tool for the determination of electromagnetic near-field distribution of optical antennas, metamaterials, and waveguides.[10–17] Using this technique, both the phase and amplitude of the near-field signal can be obtained with few 10's of nano-meter spatial resolution. Previously, antennas not coupled to a load, as well as antennas coupled to transmissions lines have been investigated with this technique.[18–24] However, to the best of our knowledge, the spatial near-field distribution of nano-antennas coupled to bolometers has not yet been explored and/or such insight used for device optimization.

In this work, using a combination of *s*-SNOM and numerical simulations, we investigate the spatial near-field distribution of single-element and arrays of dipole nano-antennas coupled to bolometers.

II. MATERIALS AND METHOD

A. Fabrication

The procedure for the fabrication of the nano-antenna-coupled bolometers has been outlined previously.[4,6] Briefly, these structures are fabricated on Si wafers having a 50 nm chromium ground plane. Roughly, 200 nm of SiO_2 is thermally deposited on the ground plane to provide for thermal and electrical isolation. The dipole nano-antenna and lead lines are made out of 100 nm-thick gold, which are patterned using electron beam lithography and lift-off. Also, a 70 nm thick niobium bolometric element is deposited by dc-sputtering after defining the pattern in an electron-beam resist layer. The position of this element is aligned across the gap between the antennas. Excess metal is removed by lift-off. Scanning electron micrographs of the single, double, and arrays of connected dipole nano-antenna-coupled microbolometers are shown in Fig. 1.

[a)]Electronic mail: gboreman@uncc.edu

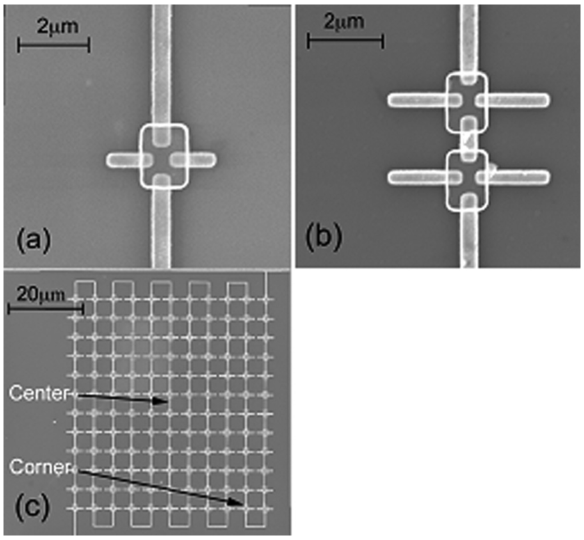

FIG. 1. SEM micrographs of the (a) single dipole nano-antenna-coupled microbolometers, (b) double dipole nano-antenna-coupled microbolometers, and (c) array of dipole nano-antenna-coupled microbolometers with annotations indicating the locations where *s*-SNOM measurements were performed.

B. Numerical simulation

Numerical simulations of the dipole nano-antenna-coupled bolometers are performed using the finite-element method (COMSOL MULTIPHYSICS). The numerical model is built using the same materials used for the fabrication and the measured optical constants for those materials at 10.6 μm.[25] The electromagnetic simulation is performed by directing a 10.6 μm wavelength and 1 V/m E-field amplitude plane wave with linear polarization matching the direction of the antenna. The resulting electrical near-field is evaluated at 100 nm over the antenna plane. Matched boundary conditions are used in the simulations and tetrahedral elements are used to discretize the computational domain.

C. *s*-SNOM and AFM measurement

The *s*-SNOM setup employs an atomic force microscope (AFM) which was modified to allow for scanning of the sample instead of the tip (Innova, Bruker). Platinum coated tips with mechanical resonance frequencies between 240 and 280 kHz are used with the AFM (Arrow-NCPt, Nanoworld). As an infrared source, a water cooled CO_2 laser provides 10.6 μm wavelength radiation (L4S, Access Laser Company).

An overview of the *s*-SNOM configuration is shown in Fig. 2, which provides a spatial resolution of approximately 50 nm and is based on the setup used previously.[10,12] Briefly, the CO_2 laser radiation is directed towards a beam splitter (BS). At the beam splitter, part of the radiation is reflected towards the sample while the other part is transmitted towards the reference mirror (RM) and quarter wave plate (QWP). The beam directed towards the sample is focused onto the tip at 60° with respect to the surface normal via a f/1 aspheric lens providing an approximately 65 μm spot focus size. The AFM is operated in tapping mode. The tip is scanned with a scan rate between 0.75 and 1.5 Hz (22.5–60 μm/s) and is adjusted according to the amount of thermal drift observed during scanning done prior to the measurement. The tip-scattered *s*-SNOM signal is collected and detected interferometrically with the beam reflected off of the RM at the mercury-cadmium-telleride (MCT) detector. In this setup, polarization selective optics, using wire grid polarizers (WGP), allows for the sample to be illuminated with predominantly s-polarized radiation while allowing to measure predominantly p-polarized scattered radiation.[22]

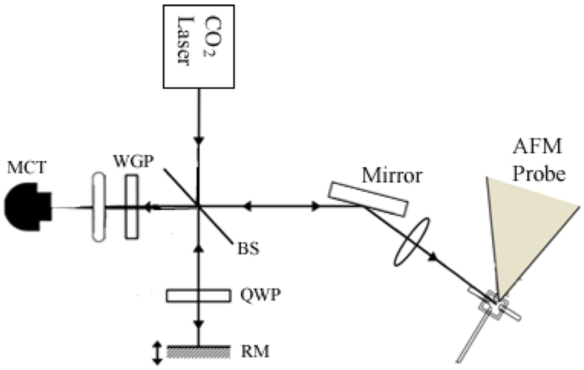

FIG. 2. Schematic showing the configuration used for the *s*-SNOM measurements.

Tapping-mode AFM height and *s*-SNOM data were collected simultaneously. The *s*-SNOM signal recorded at the detector (S_d) can approximately be expressed as

$$\begin{aligned} S_d \propto I &= |E_{scat} + E_{ref}|^2 + I_b \\ &= |E_{scat}|^2 + |E_{ref}|^2 + 2|E_{scat} \cdot E_{ref}|\cos\phi + I_b, \end{aligned} \quad (1)$$

where E_{scat} is the electric field of the scattered beam, E_{ref} is the electric field of the reference beam, φ represents the phase difference between the reference and scattered beam, and I_b is the background signal present from stray reflections and scattering not related to the scattered near-field or reference beam signal.[12,26]

A lock-in amplifier is used to extract the signal at the 2nd harmonic of the tip dither frequency, which largely eliminates the far-field background.[27,28] The RM is adjusted to change the phase difference between the two beams that recombine before reaching the detector. In order to obtain amplitude and phase images, *s*-SNOM scans are collected at different mirror positions. The images are fit, point-by-point, by a least squares cosine function to obtain the amplitude and phase information.[12,26]

The lengths of various features in the nano-antenna-coupled microbolometer structures are determined by performing cross sectional analysis of the AFM height images using WSXM version 3.1.[29]

III. RESULTS

First, tapping-mode AFM height and *s*-SNOM measurements were acquired for the single dipole nano-antenna-coupled microbolometer. Fig. 3(a) shows an AFM height

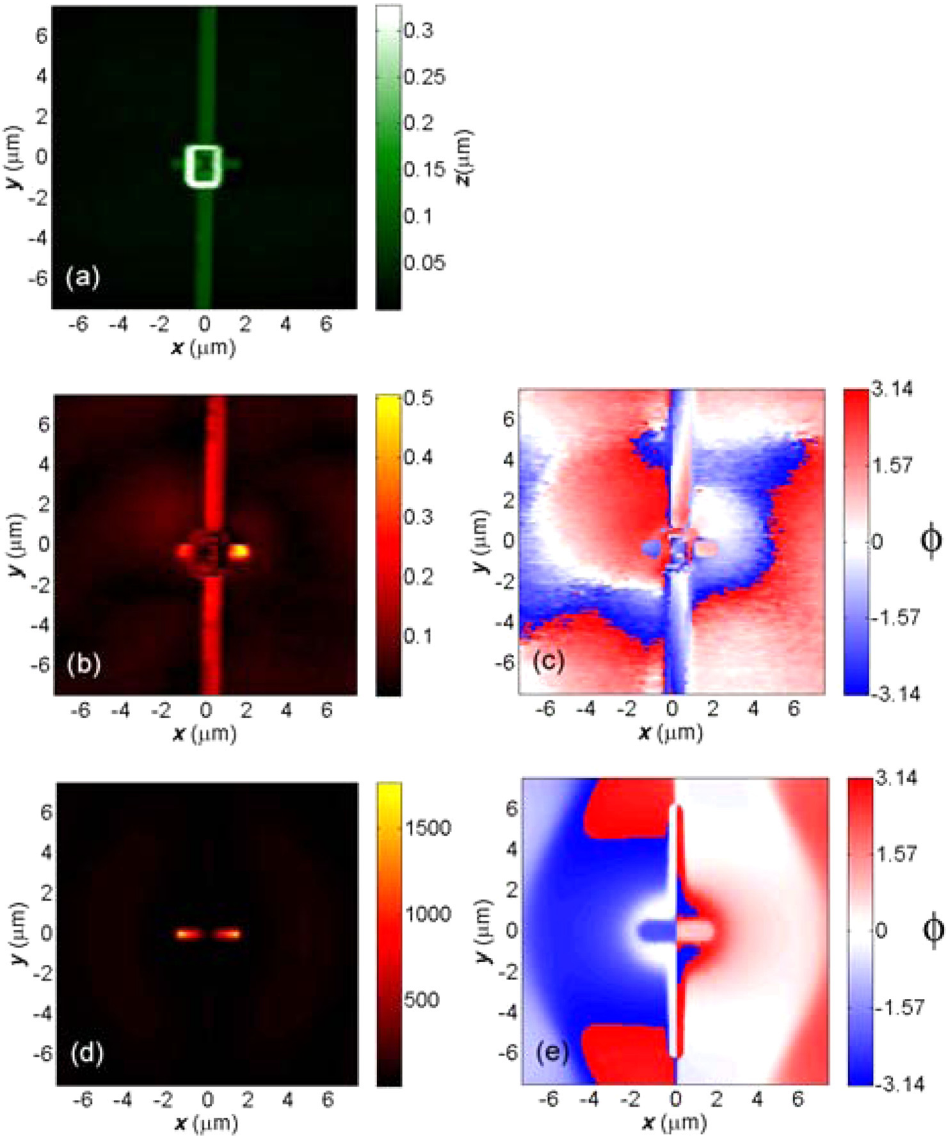

FIG. 3. Images showing simulated and measured data from the single dipole nano-antenna-coupled microbolometer structure. Shown is simultaneously recorded (a) AFM height data showing the topography of the structure, (b) measured amplitude signal from *s*-SNOM, and (c) measured phase signal from *s*-SNOM. Also shown are (d) simulated amplitude and (e) simulated phase signal calculated from COMSOL MULTIPHYSICS.

image of the single dipole nano-antenna-coupled microbolometer. The overall length of the dipole antenna structure across the two dipoles was approximately 3.3 μm when performing a cross sectional analysis of this image (not shown), which was consistent with the measured value as determined by scanning electron microscopy (SEM).

Figs. 3(b) and 3(c) show near-field amplitude and relative phase images derived from the *s*-SNOM measurements of these structures. In Fig. 3(c), the π phase difference between opposite ends of the dipoles can be seen, which was expected and has been seen in previous reports.[20,21,23,24] In Fig. 3(b), there is a slight asymmetry in the magnitude of the amplitude value on opposite ends of the pair of dipoles, which we attribute to the bolometric element being positioned slightly off center across the gap between the two dipoles. Experimentally derived amplitude images collected for other structures having different length dipoles tended to show more symmetry in the magnitude of the amplitude when the bolometric element was positioned more centrally across this gap (not shown). Figs. 3(d) and 3(e) shows COMSOL MULTIPHYSICS based simulations of the amplitude and relative phase of these structures, which qualitatively match the measured data at the dipole elements. Specifically, in both the simulation and experiment, the strongest amplitude signal of the near-field is observed towards opposite ends of the antennas. This is similar to what has been observed previously by simulation for antennas without a gap and should be expected as well with the presence of a load across a gap.[25,30] In addition, both the measured and simulated amplitude images show a minimal amount of near-field in the background (the areas around the antenna-coupled microbolometer and lead lines), although the measured and simulated phase implies some field exist in these areas. The simulated and experimental data show a difference in phase in the background [Figs. 3(c) and 3(e)], but some of this difference and the large changes in phase can be attributed to the minimal amount of field in this area, which has been shown to yield relatively large error in phase.[19] Another difference between the simulations and experimental data shown is the lack of amplitude signal from the microbolometric element and the lead lines in the simulation as compared to the experiment where a relatively strong amplitude signal is present at these structures [Figs. 3(b) and 3(d)]. Both of the above differences between the simulated and measured data

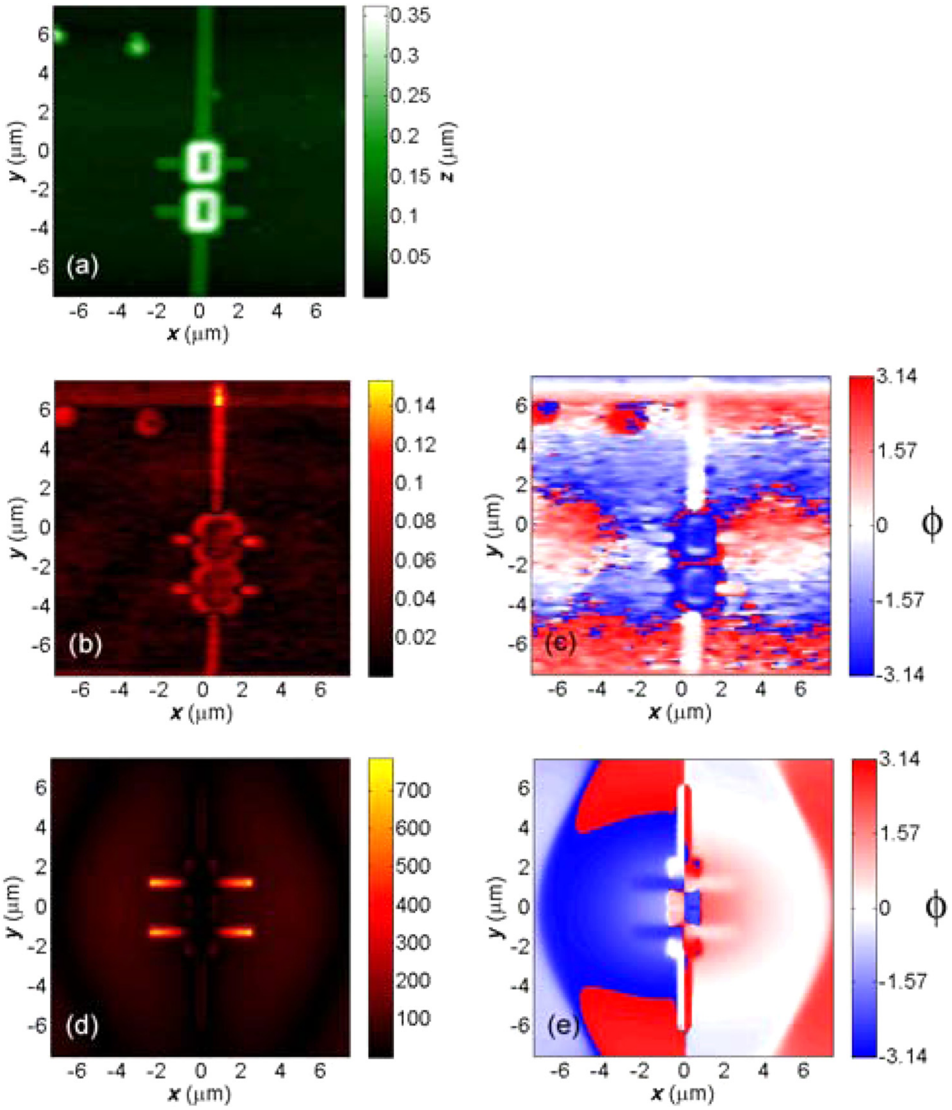

FIG. 4. Images showing simulated and measured data from the double dipole nano-antenna-coupled microbolometer structure. Shown is simultaneously recorded (a) AFM height data showing the topography of the structure, (b) measured amplitude signal from *s*-SNOM, and (c) measured phase signal from *s*-SNOM. Also shown are (d) simulated amplitude and (e) simulated phase signal calculated from COMSOL MULTIPHYSICS.

can be mostly attributed to the simulations being performed by exciting the structures with the incident radiation normal to the surface plane while in the experiment the structures were excited with the incident radiation at 60° off normal. This leads to *s*-SNOM dielectric material contrast due to the tip-sample coupling.

Next, tapping-mode AFM height and *s*-SNOM measurements were acquired for the double dipole nano-antenna-coupled microbolometer. Fig. 4(a) shows an AFM height image of the double dipole nano-antenna-coupled microbolometer. Cross sectional analysis of this image showed that the overall length of the dipole antenna structure across the two dipoles was approximately 4.5 μm, while the separation between the antennas from the different antenna-coupled microbolometer structures was approximately 1.6 μm (not shown). Both these values were consistent with measurements done by SEM.

Figs. 4(b) and 4(c) show amplitude and relative phase images derived from the *s*-SNOM measurement of these structures. As with the single dipole nano-antenna-coupled microbolometer structure, the expected π phase difference between the ends of the dipoles can be seen in Fig. 4(c), although it is not as clearly evident. Here, the amplitude of the near-field is more symmetric on opposite ends of the dipoles, which is likely due to the bolometric element being positioned more centrally across the gap between the dipoles compared with the single dipole-coupled microbolometer. Figs. 4(d) and 4(e) show corresponding COMSOL simulations of the amplitude and relative phase of these structures. Although the key resonant features observed are reproduced in the calculations, the experimental signal is dominated by background and contrast from the dipole antenna, the microbolometric element, and the lead lines [Figs. 4(b) and 4(d)].

In the next set of measurements shown in Figs. 5 and 6, tapping-mode AFM height and *s*-SNOM measurements were acquired for the array of connected dipole nano-antenna-coupled microbolometers. A SEM image of the full array is shown in Fig. 1(c) above, which shows the locations in the array where the measurements were performed. Measurements were taken in two different regions of the array. Figs. 5(a) and 6(a) shows AFM height images of the array of dipole nano-antenna-coupled microbolometer at the corner of the array and center of the array, respectively. Cross sectional analysis of

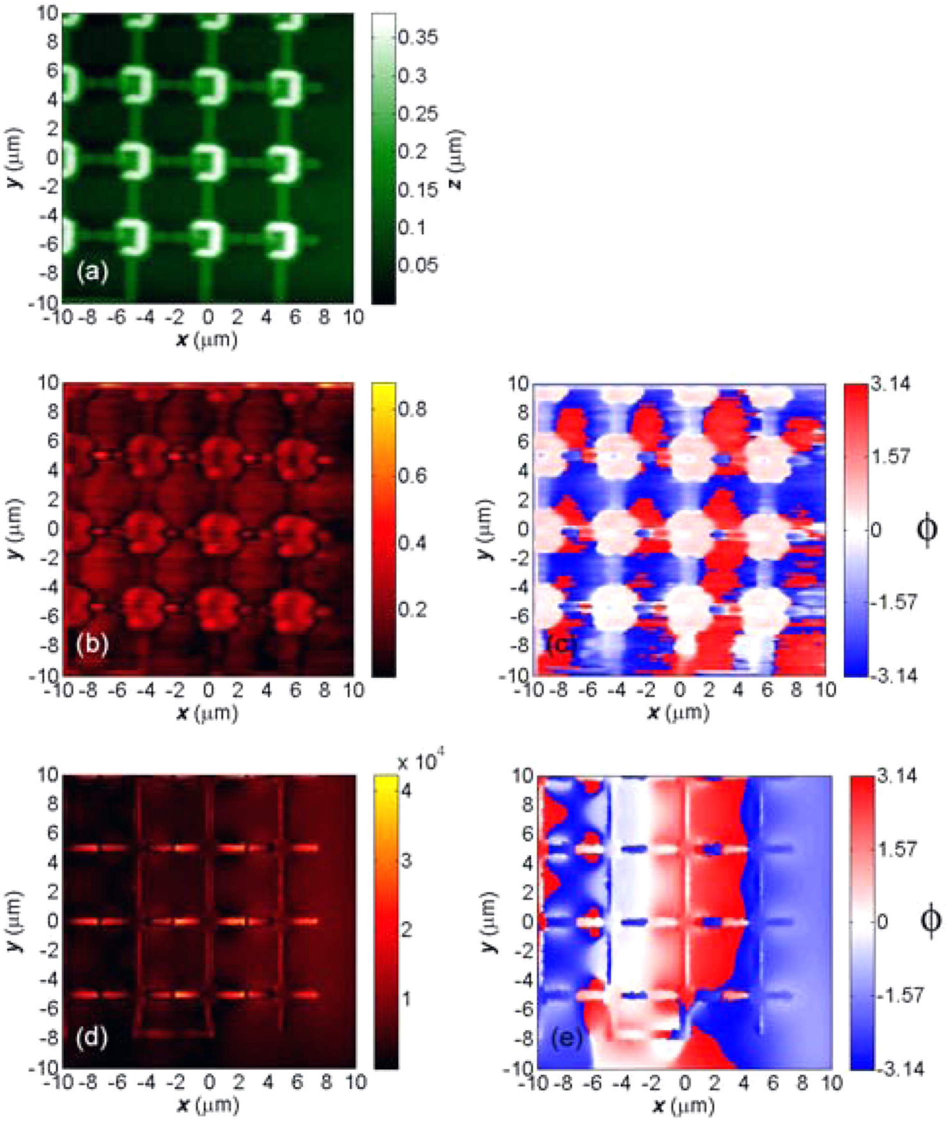

FIG. 5. Images showing simulated and measured data from the corner of the dipole nano-antenna-coupled microbolometer array structure. Shown is simultaneously recorded (a) AFM height data showing the topography of the structure, (b) measured amplitude signal from *s*-SNOM, and (c) measured phase signal from *s*-SNOM. Also shown are (d) simulated amplitude and (e) simulated phase signal calculated from COMSOL MULTIPHYSICS.

these images showed that the overall length of the dipole antenna structure across the two dipoles in the array was approximately 5 μm (not shown). In this analysis, the separation between the antennas from the different antenna-coupled microbolometer structures in the y-direction in the image was approximately 5 μm, while the gap between adjacent dipoles belonging to different sensing elements was approximately 0.5 μm (along the x-direction). All these values derived from the AFM height images were consistent with the measured values determined by SEM.

Figs. 5(b) and 5(c) show amplitude and relative phase images derived from the *s*-SNOM measurement of these structures in the corner of the array, while Figs. 6(b) and 6(c) show amplitude and relative phase images from near the center of the array. As with the previous single and double dipole coupled microbolometer structures, Figs. 5(c) and 6(c) show a π phase difference between the ends of the dipoles at both locations in the array. However, the amplitude image from the center of the array [Fig. 6(b)] shows more asymmetry in the strength of the amplitude of the near-field at opposite ends of the dipoles compared to the amplitude image for the corner of the array [Fig. 5(b)]. As with the single dipole coupled microbolometer, this asymmetry in the amplitude signal at the center of the array could be due to the bolometric element in the experiment being positioned more off center across the gap between the two dipoles.

Figs. 5(d) and 5(e) show corresponding COMSOL simulations of the amplitude and relative phase at the corner of the array, while Figs. 6(d) and 6(e) show simulations of the amplitude and relative phase at near the center of the array. The simulation of the phase for both areas of the array [Figs. 5(e) and 6(e)] is consistent with measured data mentioned above where a π phase shift is also observed across the opposite ends of the dipoles. Also, the simulation of the amplitude at the corner of the array shows near equal strengths in the amplitude signal at the opposite ends of the dipoles, which is consistent with the measured data shown in Fig. 5(b). The simulation of the amplitude signal at the center of the array shows more symmetry in the strength of the amplitude signal at the ends of the dipoles compared to the measured data [Fig. 6(b)], which further supports that the amplitude of the near-field in these areas is sensitive to the position of the bolometric element relative to the dipoles.

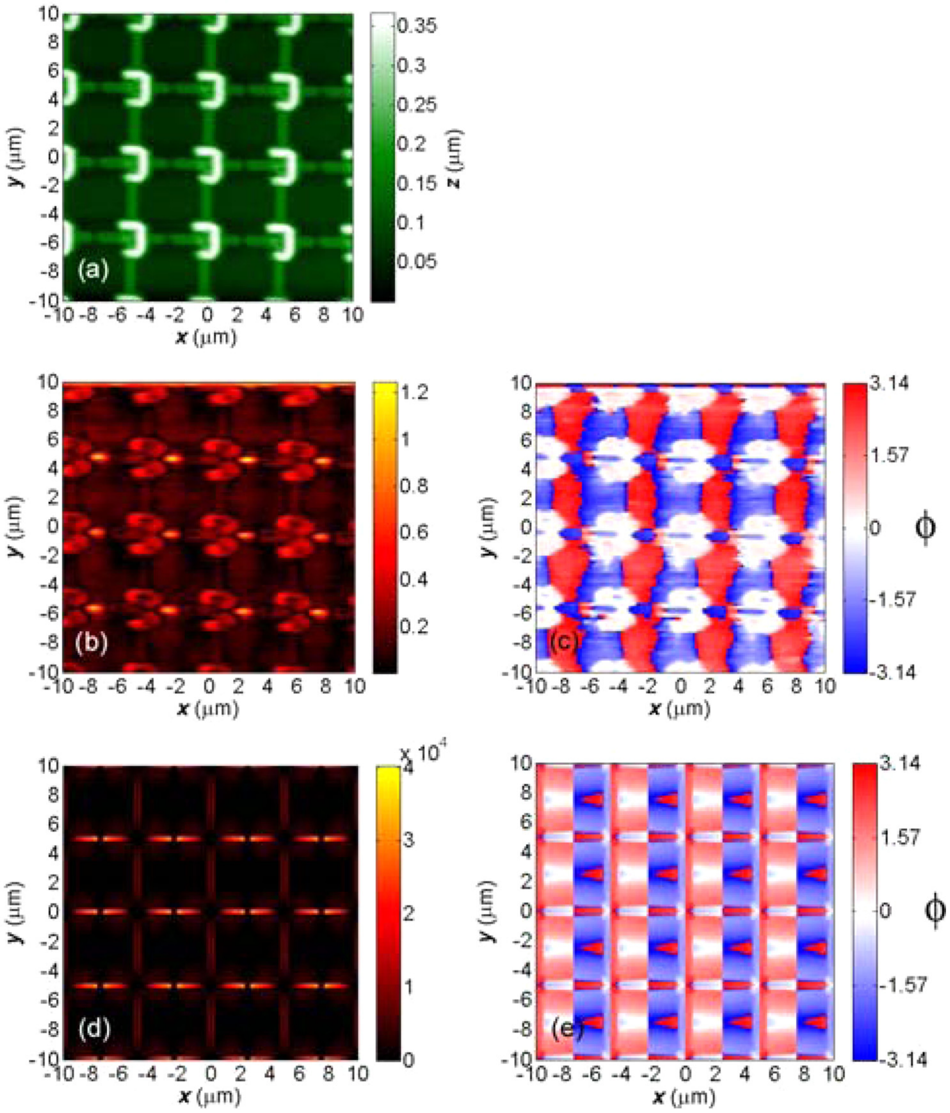

FIG. 6. Images showing simulated and measured data from the inside region of the dipole nano-antenna coupled microbolometer array structure. Shown is simultaneously recorded (a) AFM height data showing the topography of the structure, (b) measured amplitude signal from *s*-SNOM, and (c) measured phase signal from *s*-SNOM. Also shown are (d) simulated amplitude and (e) simulated phase signal calculated from COMSOL MULTIPHYSICS.

IV. CONCLUSION

In this work, the near-field characterization of dipole antenna-coupled microbolometers is obtained experimentally and by finite-element simulations. In most cases, both experimentally derived phase and amplitude images of the near-field signal qualitatively match simulations performed using COMSOL MULTIPHYSICS and are consistent with classical antenna theory. Specifically, the expected π phase shift across the length of the antenna elements is observed for all the structures in the experiment as well as in the simulations. Interestingly, the amplitude of the near-field signal on opposite ends of the antenna elements is approximately equal depending on how well the bolometric element is centered on top of the dipole antennas. The effect of the position of the bolometric element on the amplitude signal on the antenna arms suggests that energy will be coupled differently into this element depending on the relative position of these structures and this could have a significant impact on the response of these types of detectors.

The results presented in this work are relevant for the use of the near-field in nano-antennas for integrated optics applications and for utilizing the phase coupling of these antennas in order to design nano-antenna-phase arrays for beam steering applications.[31,32]

Future work will examine single dipole nano-antenna-coupled microbolometer structures of different overall lengths across the dipole and study the effect that different length structures have on the resulting near-field distributions. The first resonance length of these structures was predicted to be roughly 3.1 μm in a previous report,[4] which is smaller than the length of these structures ($\sim$3.3 μm). However, it has been shown that dipole behavior can still be observed for antennas with lengths greater than the resonance length,[22] which is what we have observed in this report.

ACKNOWLEDGMENTS

We would like to acknowledge Dr. Ed Kinzel for helpful discussions.

[1] V. Y. Zerov, V. G. Malyarov, and I. A. Khrebtov, J. Opt. Technol. **78**, 308–316 (2011).
[2] S. E. Schwarz and B. T. Ulrich, J. Appl. Phys. **48**, 1870–1873 (1977).

[3]R. A. Wood, in *Electron Devices Meeting, 1993. IEDM '93. Technical Digest., International* (1993), pp. 175–177.

[4]F. J. González and G. D. Boreman, Infrared Phys. Technol. **46**, 418–428 (2005).

[5]I. Codreanu and G. D. Boreman, Appl. Opt. **41**, 1835–1840 (2002).

[6]F. J. González, C. S. Ashley, P. G. Clem, and G. D. Boreman, Infrared Phys. Technol. **45**, 47–51 (2004).

[7]C. Fumeaux, M. A. Gritz, I. Codreanu, W. L. Schaich, F. J. González, and G. D. Boreman, Infrared Phys. Technol. **41**, 271–281 (2000).

[8]F. J. González, B. Ilic, J. Alda, and G. D. Boreman, IEEE J. Sel. Top. Quantum Electron. **11**, 117–120 (2005).

[9]N. Chong and H. Ahmed, Appl. Phys. Lett. **71**, 1607 (1997).

[10]A. C. Jones, R. L. Olmon, S. E. Skrabalak, B. J. Wiley, Y. N. Xia, and M. B. Raschke, Nano Lett. **9**, 2553–2558 (2009).

[11]T. Taubner, F. Keilmann, and R. Hillenbrand, Opt. Express **13**, 8893–8899 (2005).

[12]E. C. Kinzel, J. C. Ginn, R. L. Olmon, D. J. Shelton, B. A. Lail, I. Brener, M. B. Sinclair, M. B. Raschke, and G. D. Boreman, Opt. Express **20**, 11986–11993 (2012).

[13]A. Garcia-Etxarri, I. Romero, F. J. Garcia de Abajo, R. Hillenbrand, and J. Aizpurua, Phys. Rev. B **79**, 125439 (2009).

[14]F. Keilmann and R. Hillenbrand, Philos. Trans. R. Soc. London, Ser. A **362**, 787–806 (2004).

[15]M. Rang, A. C. Jones, F. Zhou, Z.-Y. Li, B. J. Wiley, Y. Xia, and M. B. Raschke, Nano Lett. **8**, 3357–3363 (2008).

[16]T. Zentgraf, J. Dorfmüller, C. Rockstuhl, C. Etrich, R. Vogelgesang, K. Kern, T. Pertsch, F. Lederer, and H. Giessen, Opt. Lett. **33**, 848–850 (2008).

[17]P. Alonso-Gonzalez, M. Schnell, P. Sarriugarte, H. Sobhani, C. Wu, N. Arju, A. Khanikaev, F. Golmar, P. Albella, L. Arzubiaga, F. Casanova, L. E. Hueso, P. Nordlander, G. Shvets, and R. Hillenbrand, Nano Lett. **11**, 3922–3926 (2011).

[18]P. M. Krenz, R. L. Olmon, B. A. Lail, M. B. Raschke, and G. D. Boreman, Opt. Express **18**, 21678–21686 (2010).

[19]L. A. Florence, E. C. Kinzel, R. L. Olmon, J. C. Ginn, M. B. Raschke, and G. D. Boreman, Infrared Phys. Technol. **55**, 449–553 (2012).

[20]R. Hillenbrand, in *36th International Conference on Infrared, Millimeter and Terahertz Waves (IRMMW-THz)* (2011), pp. 1–3.

[21]M. Schnell, P. Alonso Gonzalez, L. Arzubiaga, F. Casanova, L. E. Hueso, A. Chuvilin, and R. Hillenbrand, Nat. Photonics **5**, 283–287 (2011).

[22]R. L. Olmon, P. M. Krenz, A. C. Jones, G. D. Boreman, and M. B. Raschke, Opt. Express **16**, 20295–20305 (2008).

[23]P. Sarriugarte, M. Schnell, P. Alonso-Gonzalez, L. Arzubiaga, F. Golmar, F. Casanova, L. E. Hueso, and R. Hillenbrand, Opt. Commun. **285**, 3378–3382 (2012).

[24]P. Alonso-Gonzalez, P. Albella, F. Golmar, L. Arzubiaga, F. Casanova, L. E. Hueso, J. Aizpurua, and R. Hillenbrand, Opt. Express **21**, 1270–1280 (2013).

[25]F. J. González, J. Alda, J. Simon, J. Ginn, and G. Boreman, Infrared Phys. Technol **52**, 48–51 (2009).

[26]B. Deutsch, R. Hillenbrand, and L. Novotny, Opt. Express **16**, 494–501 (2008).

[27]R. Hillenbrand and F. Keilmann, Phys. Rev. Lett. **85**, 3029–3032 (2000).

[28]B. Knoll and F. Keilmann, Opt. Commun. **182**, 321–328 (2000).

[29]I. Horcas, R. Fernandez, J. M. Gomez-Rodriguez, J. Colchero, J. Gomez-Herrero, and A. M. Baro, Rev. Sci. Instrum. **78**, 013705-8 (2007).

[30]H. Paolo Biagioni, J.-S. Huang, and H. Bert, Rep. Prog. Phys. **75**, 024402 (2012).

[31]F. J. Gonzalez and J. Alda, in *Proceedings of the Fourth European Conference on Antennas and Propagation (EuCAP)* (2010), pp. 1–3.

[32]D. Dregely, R. Taubert, J. Dorfmuller, R. Vogelgesang, K. Kern, and H. Giessen, Nat. Commun. **2**, 267 (2011).